JOURNAL OF GUIDANCE, CONTROL, AND DYNAMICS
Vol. 25, No. 4, July–August 2002

Optimization of Vertical Plane Cobralike Pitch Reversal Maneuvers

H. J. Komduur* and H. G. Visser†
Delft University of Technology, 2600 GB Delft, The Netherlands

Four time-optimal, vertical plane, cobralike pitch maneuvers corresponding to different sets of boundary conditions have been studied for the F-18 high-angle-of-attack research vehicle aircraft. These maneuvers are poststall maneuvers that enable an aircraft that is initially followed by a pursuing aircraft to shift positions, that is, the initial evader turns into the pursuer. The initial pursuer is assumed to remain at constant speed and altitude. In addition an 80-deg pitch reversal maneuver has been considered that was optimized using a Chebyshev approach. A nonlinear programming and collocation method was successfully used to find the optimal vertical plane trajectories in open-loop form. All trajectories that were found have been put through a six-degree-of-freedom simulation utilizing a nonlinear inversion closed-loop control technique. The results showed that the optimal vertical plane trajectories can be flown quite accurately, using longitudinal and lateral thrust vectoring, along with the conventional aerodynamic controls.

Nomenclature

b	=	reference span, ft
C_D	=	drag coefficient
C_L	=	lift coefficient
C_l	=	rolling moment coefficient
C_m	=	pitching moment coefficient
C_{m0}	=	basic pitching moment coefficient
C_n	=	yawing moment coefficient
C_X	=	longitudinal force coefficient
C_Y	=	side-force coefficient
C_Z	=	normal force coefficient
$\bar{c}$	=	reference mean aerodynamic chord, ft
g	=	acceleration of gravity, ft/s^2
H	=	altitude, ft
I_{xx}	=	moment of inertia around the roll axis, lb $\cdot$ ft^2
I_{xz}	=	cross product of inertia between roll and yaw axes, lb $\cdot$ ft^2
I_{yy}	=	moment of inertia around the pitch axis, lb $\cdot$ ft^2
I_{zz}	=	moment of inertia around the yaw axis, lb $\cdot$ ft^2
l_X	=	distance from nozzle exit to center of gravity, ft
M	=	vehicle mass, lb
p	=	roll rate, rad/s
q	=	pitch rate, rad/s
$\bar{q}$	=	dynamic pressure, $0.5\rho V^2$, psi
r	=	yaw rate, rad/s
S	=	reference surface area, ft^2
$T_{X,Y,Z}$	=	body-axis components of thrust, lbf
t	=	time, s
V	=	aircraft true airspeed, ft/s
α	=	angle of attack, rad
β	=	sideslip angle
γ	=	flight path angle, rad
δ_a	=	aileron deflection, deg
δ_e	=	elevator deflection, deg
δ_r	=	rudder deflection, deg
δ_y	=	lateral thrust vectoring angle, deg
δ_z	=	longitudinal thrust vectoring angle, deg
θ	=	pitch angle, rad
ρ	=	air density, lb/ft^3
φ	=	bank angle, rad
χ	=	heading angle, rad
ψ	=	yaw angle, rad

Subscripts

c	=	commanded
d	=	desired
e	=	end
f	=	final value
p	=	derivative with respect to roll rate, s/rad
q	=	derivative with respect to pitch rate, s/rad
r	=	derivative with respect to yaw rate, s/rad
β	=	derivative with respect to sideslip angle, 1/deg
δ_a	=	derivative with respect to aileron deflection, 1/deg
δ_e	=	derivative with respect to elevator deflection, 1/deg
δ_r	=	derivative with respect to rudder deflection, 1/deg
0	=	start value

Received 12 July 2001; revision received 15 December 2001; accepted for publication 20 February 2002.

*M.Sc. Student, Faculty of Aerospace Engineering, Department of Flight Mechanics and Propulsion, P.O. Box 5058; currently Research Associate, Rocket Technology, TNO Prins Maurits Laboratory, 2280 AA Rijswijk, The Netherlands; komduur@pml.tno.nl. Member AIAA.

†Lecturer, Faculty of Aerospace Engineering, Department of Flight Mechanics and Propulsion, P.O. Box 5058; H.G.Visser@lr.tudelft.nl. Associate Fellow AIAA.

Introduction

FLIGHT tests conducted in 1994 verified that the application of thrust vectoring (TV) in air combat engagements gives the aircraft that is equipped with it a definite edge over conventional adversaries during close-in combat. For example, in mock-dogfights, a TV-equipped X-31 flying against a conventional F/A-18 produced a kill ratio[1] of 32:1. TV technology gives the aircraft the capability to fly at angles of attack (AOA) beyond the stall AOA, the AOA at maximum lift coefficient. An example of such a poststall maneuver is the Pougachev cobra maneuver, first demonstrated by a Sukhoi Su-27 at the Paris Air Show in 1989.[2] During this maneuver, the aircraft rapidly pitches up to about 100–120 deg. In other words, the aircraft is flying tail first. The tremendous amount of drag in the poststall region causes the aircraft to slow down rapidly from an initial 400 ft/s to about 100–130 ft/s, after which the aircraft pitches down again. The maneuver was named after its resemblance to an attacking cobra snake.

Several additional maneuvers that make use of TV have been proposed.[3] In this paper cobralike poststall pitch reversal maneuvers will be studied. A simplification often made while optimizing these maneuvers is that the fast body dynamics of the aircraft are ignored,

that is, pitching movements about the body Y axis are simplified by ignoring moments of inertia. In this study, the effects of the moments of inertia are taken into account in the optimization of the maneuvers in the vertical plane. The optimal open-loop trajectories will be studied further by putting them in a simulator utilizing nonlinear inversion closed-loop control to see whether they are flyable, that is, can be closely tracked, using a complete six-degree-of-freedom (DOF) model.

Problem Formulation

One of the problems implemented in this study was the cobra maneuver in an evader–pursuer form that was first presented by Murayama and Hull,[4] and studied further by Horie and Conway.[5] The initial pursuer is in-flight at constant speed and constant altitude. The initial evader is the F-18 high-angle-of-attack research vehicle (HARV), capable of poststall flight. (The F-18 HARV was built before the F-18 was redesignated F/A-18.) The initial invader starts out 1000 ft ahead of the initial pursuer. The objective of the initial evader is to become the pursuer, that is, shift positions with the initial pursuer, in minimum time. At the final time, the initial evader is 1000 ft behind the initial pursuer. The maneuver is shown in Fig. 1.

Only initial and end conditions are formulated, namely,

$$\gamma_0 = \gamma_f = 0 \tag{1}$$

Because

$$\theta = \gamma + \alpha \tag{2}$$

and γ is not part of the state vector, constraint (1) is translated to

$$\theta_0 = \alpha_0 \tag{3}$$

$$\theta_f = \alpha_f \tag{4}$$

Furthermore,

$$q_0 = 0 \tag{5}$$

$$V_0 = 400 \tag{6}$$

$$H_0 = 10{,}000 \tag{7}$$

$$X_0 = 1000 \tag{8}$$

$$X_f = V_0 t_f - 1000 \tag{9}$$

The latter two conditions imply that the maneuvering aircraft starts out 1000 ft ahead of the enemy fighter, although it ends up 1000 ft behind it. The goal is to minimize the objective function J:

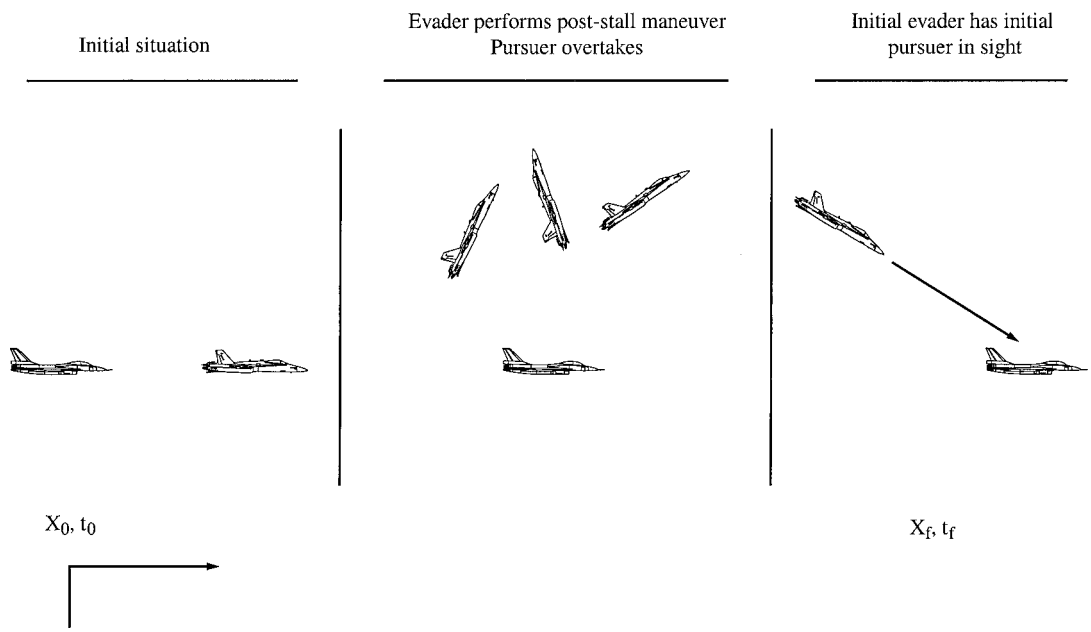

Fig. 1 Graphical representation of the evasive–offensive maneuver.

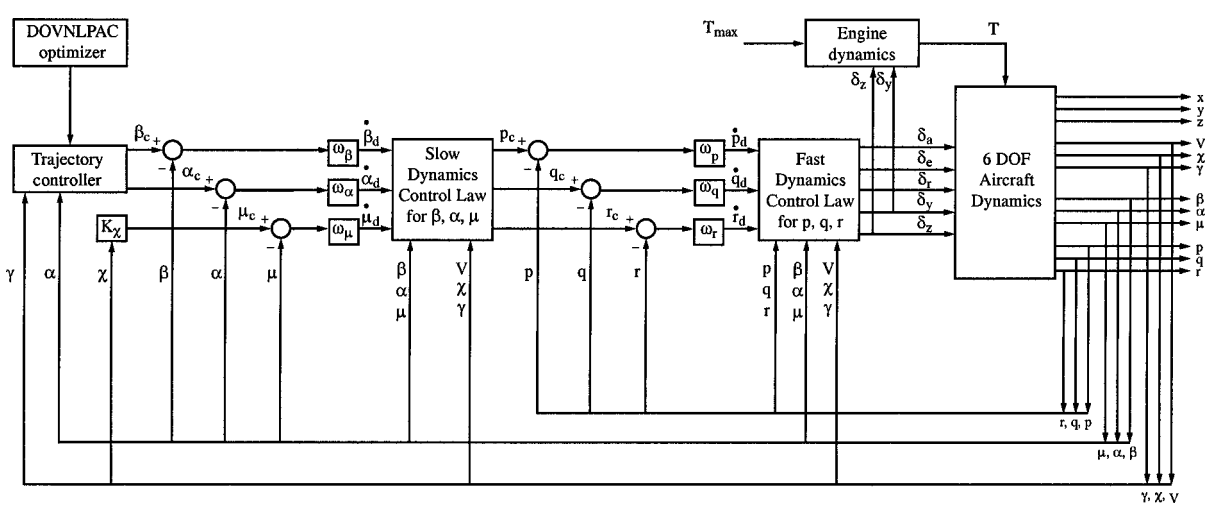

Fig. 2 Configuration of nonlinear dynamic inversion laws.

$$J = t_f \tag{10}$$

In words, the aircraft tries to get from in front of to behind the enemy fighter in minimum time.

Several cases were examined, using a method similar to that of Horie and Conway.[5] In their paper, they formulated additional constraints to the original problem formulated by Murayama and Hull.[4] In the present study, the problem is first examined using just the horizontal distance constraint formulated in Eq. (9). In the second case that is examined, a pointing constraint and a total distance constraint as formulated by Horie and Conway[5] are introduced. The pointing constraint states that at the final time the nose of the initial evader is pointed toward the initial pursuer. Moreover, there should be at least a 1000-ft separation between the two aircraft. This is done to ensure that the initial pursuer is in sight of the pilot of the initial evader and is not obscured by the aircraft's nose. The mathematical formulation of these constraints is as follows:

$$\sqrt{(V_0 t_f - X_0)^2 + (H_0 - H_f)^2} \geq 1000 \tag{11}$$

which is called the total distance constraint, and

$$\sqrt{(V_0 t_f - X_0)^2 + (H_0 - H_f)^2} = \cos\theta_f (V_0 t_f - X_f) + \sin\theta_f (H_0 - H_f) \tag{12}$$

which will be called the pointing constraint. In this case, constraint (4) is dropped, that is, the final flight-path angle is no longer required to be zero. In the third case that is considered, a constraint is imposed on the speed of the aircraft at the final time. During poststall maneuvering a lot of energy is lost. This influences the aircraft's capability to engage another target after the first pursuer has been eliminated. Therefore, the speed of the aircraft at the final time is required to be the same as the initial speed:

$$V_e = V_0 = 400 \tag{13}$$

The fourth case considered in the evader–pursuer scenario is when the final flight-path angle is forced to be zero. This is done to ensure that the initial evader is able to follow the initial pursuer:

$$\gamma_f = \theta_f - \alpha_f = 0 \rightarrow \theta_f = \alpha_f \tag{14}$$

Another form of the cobra maneuver is the 80-deg pitch reversal described by Lichtsinder et al.[6] The objective is to pitch up the aircraft from an initial

$$\theta_0 = 0, \qquad \dot{\theta}_0 = 0 \tag{15}$$

to

$$\theta = 80, \qquad \dot{\theta} = 0 \tag{16}$$

and back to

$$\theta_f = 0, \qquad \dot{\theta}_f = 0 \tag{17}$$

This is to be accomplished in minimum time.

Lichtsinder et al.[6] split the maneuver into two separate parts, that is, a to-target phase and a recovery phase. In essence, these

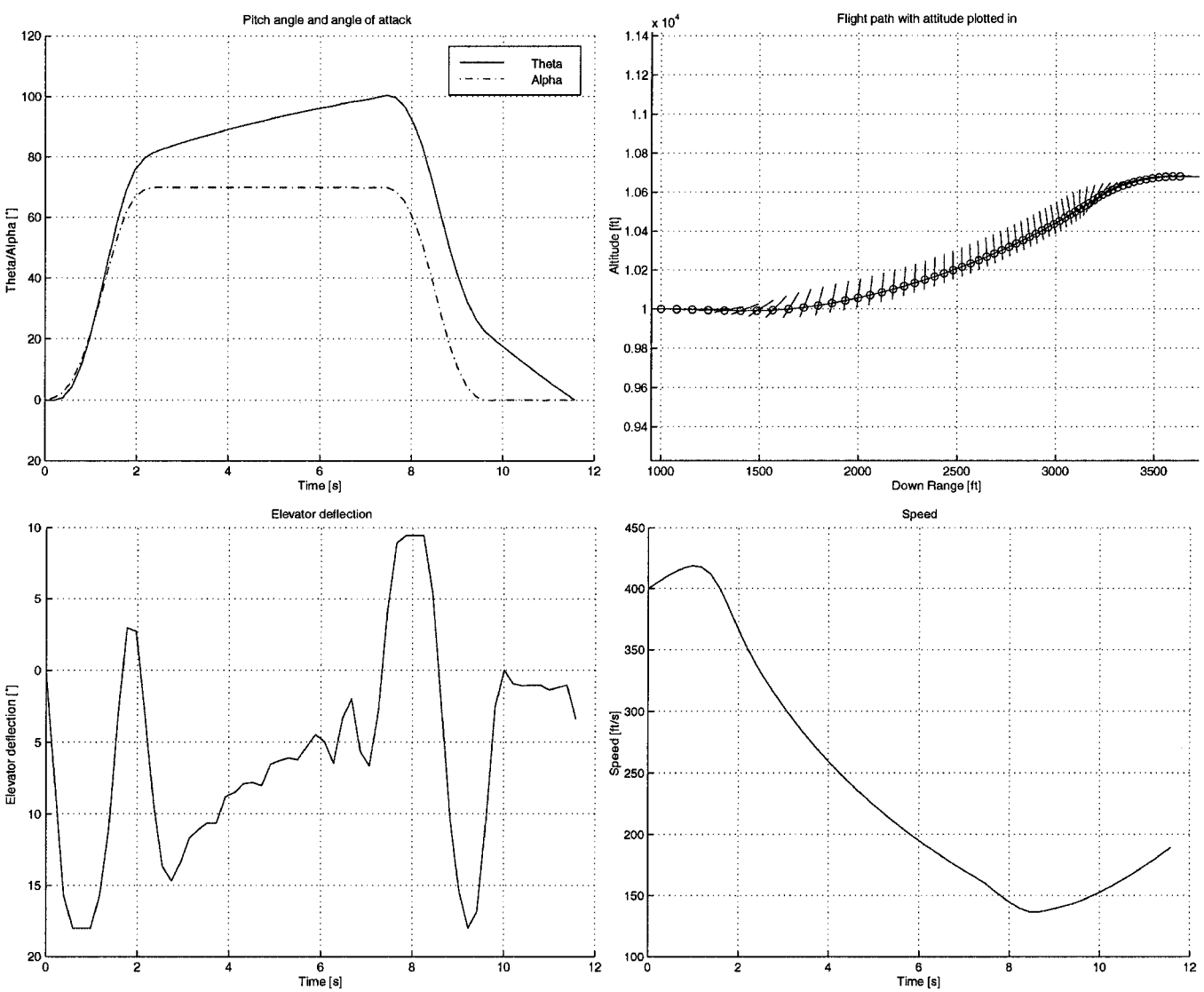

Fig. 3 Evader–pursuer maneuver, horizontal distance constraint only.

are two separate maneuvers. That the problem is split in two may have implications for overall optimality. Therefore, in this study, a Chebyshev approach is used. The problem is transformed to a fixed-time max–max problem, that is, maximizing the maximum value of θ during a given maneuvering time, with

$$\theta_0 = \alpha_0 = 0, \qquad \theta_f = \alpha_f = 0 \tag{18}$$

$$q_0 = 0 \tag{19}$$

$$V_0 = 400 \tag{20}$$

$$H_0 = 10{,}000 \tag{21}$$

$$X_0 = 0 \tag{22}$$

The original objective function has been approximated as follows:

$$J = \int_{t_0}^{t_f} -(\theta)^K \, \mathrm{d}t \tag{23}$$

where K has a sufficiently large value, for instance, $K = 10$ or 20 (Ref. 7). In the present study, choosing a value for K as large as 44 was possible. The specified maneuvering time was subsequently gradually reduced from an initial 7 s such that an 80-deg pitch reversal was ultimately obtained.

Physical Model

The point-mass model used by both Murayama et al.[4] and Horie and Conway[5] has three DOF and uses AOA or AOA and longitudinal TV for control variables, respectively. Moments of inertia around the Y axis are completely ignored, and therefore, the rate of change of AOA is unbounded.

In this study, a rigid-body model is used. The elevator deflection δ_e is the control variable. Along with this, the longitudinal deflection of thrust is used. Thrust deflection is assumed to be slaved to the elevator deflection through a linear scheme such that at maximum elevator deflection the thrust deflection is maximal as well. Similarly, if elevator deflection is zero, thrust deflection is also zero. This scheme is very simplistic; however, it does serve as a useful model during the optimization phase of the study. Later, the optimum trajectory was put in a simulator that utilized a nonlinear inversion technique, to try to let the aircraft fly along the optimum trajectory. During these simulation experiments, this linear scheme was dropped, and the elevator and the longitudinal TV vanes were able to move independently from one another. Although it would be impractical to introduce separate controls for TV and elevator deflection into the cockpit, this decoupling provides insight into control behavior that may prove useful in autopilot design. Thrust is kept at maximum afterburner throughout the maneuver, to provide maximum TV-induced moments on the aircraft. The influence of Mach number on thrust is neglected because the maneuver takes place at low speed. However, thrust loss due to TV has been modeled.[8] The variation of air density is based on the International Standard Atmosphere.

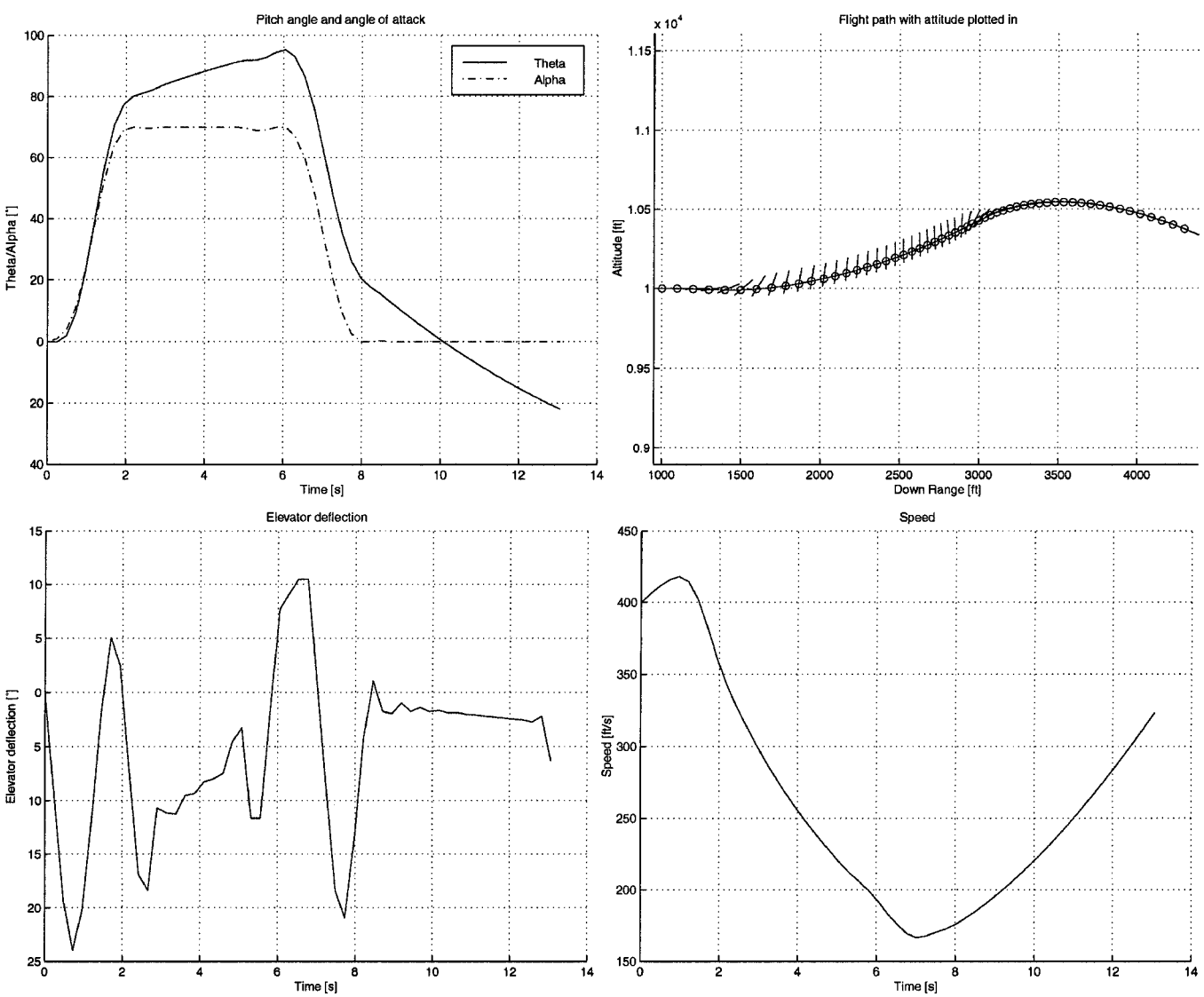

Fig. 4 Evader–pursuer maneuver, pointing and total distance constraints.

Restrictions that have been imposed during the maneuver are

$$0 \leq \alpha \leq 70 \tag{24}$$

because the available aerodynamic database of the aircraft model only covers these angles of attack. Furthermore, both rate and deflection limits for the elevator control surface have been assumed.

The six-DOF equations of motion used in the present study are the same as those used by Lichtsinder et al.[6] The model describes a high-performance fighter aircraft, with state vector $[\alpha, \beta, p, q, r, V, \psi, \theta, \phi]$ and control vector $[\delta_a, \delta_e, \delta_r, \delta_y, \delta_z]$. This means that use is made neither of the ability to roll using differential longitudinal TV on the engines nor of the leading- and trailing-edge flaps. The model consists of the following equations:

$$\dot{\alpha} = q + \{-[\bar{q}SC_X/MV - (g/V)\sin\theta + r\sin\beta]\sin\alpha + [\bar{q}SC_Z/MV - (g/V)\cos\theta\cos\varphi - p\sin\beta]\cos\alpha\}\sec\beta \tag{25}$$

$$\dot{\beta} = -\{[\bar{q}SC_X/MV - (g/V)\sin\theta]\sin\beta + r\}\cos\alpha + [\bar{q}SC_Y/MV + (g/V)\cos\theta\sin\varphi]\cos\beta - \{[\bar{q}SC_Z/MV + (g/V)\cos\theta\cos\varphi]\sin\beta - p\}\sin\alpha \tag{26}$$

$$\dot{p} = \left\{-\left[(I_{zz} - I_{yy})/I_{xx} + I_{xz}^2/I_{xx}I_{zz}\right]qr + [1 - (I_{yy} - I_{xx})/I_{zz}]I_{xz}pq/I_{xx} + \bar{q}Sb/I_{xx}(C_l + I_{xz}C_n/I_{zz})\right\}\Big/\left(1 - I_{xz}^2/I_{xx}I_{zz}\right) \tag{27}$$

$$\dot{q} = \bar{q}S\bar{c}C_m/I_{yy} + [(I_{zz} - I_{xx})/I_{yy}]pr + I_{xz}(r^2 - p^2)\big/I_{yy} \tag{28}$$

$$\dot{r} = \left\{\left[I_{xz}^2/I_{xx}I_{zz} - (I_{yy} - I_{xx})/I_{zz}\right]pq - [1 + (I_{zz} - I_{yy})/I_{xx}](I_{xz}/I_{zz})qr + \bar{q}Sb/I_{zz}((I_{xz}/I_{xx})C_l + C_n)\right\}\Big/\left(1 - I_{xz}^2/I_{xx}I_{zz}\right) \tag{29}$$

$$\dot{V} = (\bar{q}SC_X/M - g\sin\theta)\cos\alpha\cos\beta + (\bar{q}SC_Y/M + g\cos\theta\sin\varphi)\sin\beta + (\bar{q}SC_Z/M + g\cos\theta\cos\varphi)\sin\alpha\cos\beta \tag{30}$$

$$\dot{\psi} = q\sin\varphi\sec\theta + r\cos\varphi\sec\theta \tag{31}$$

$$\dot{\theta} = q\cos\varphi - r\sin\varphi \tag{32}$$

$$\dot{\varphi} = p + r\cos\varphi\tan\theta + q\sin\varphi\tan\theta \tag{33}$$

$$C_X = C_L(\alpha, q, \delta_e)\sin\alpha - C_D(\alpha, \delta_e)\cos\alpha + T_X/\bar{q}S \tag{34}$$

$$C_Y = C_{Y\delta r}(\alpha)\delta_r + C_{Y\delta a}(\alpha)\delta_a + C_{Y\delta e}(\alpha)\delta_e + C_{Y\beta}(\alpha)\beta + (b/2V)[C_{Yp}(\alpha)p + C_{Yr}(\alpha)r] + T_Y/\bar{q}S \tag{35}$$

$$C_Z = -C_L(\alpha, q, \delta_e)\cos\alpha - C_D(\alpha, \delta_e)\sin\alpha + T_Z/\bar{q}S \tag{36}$$

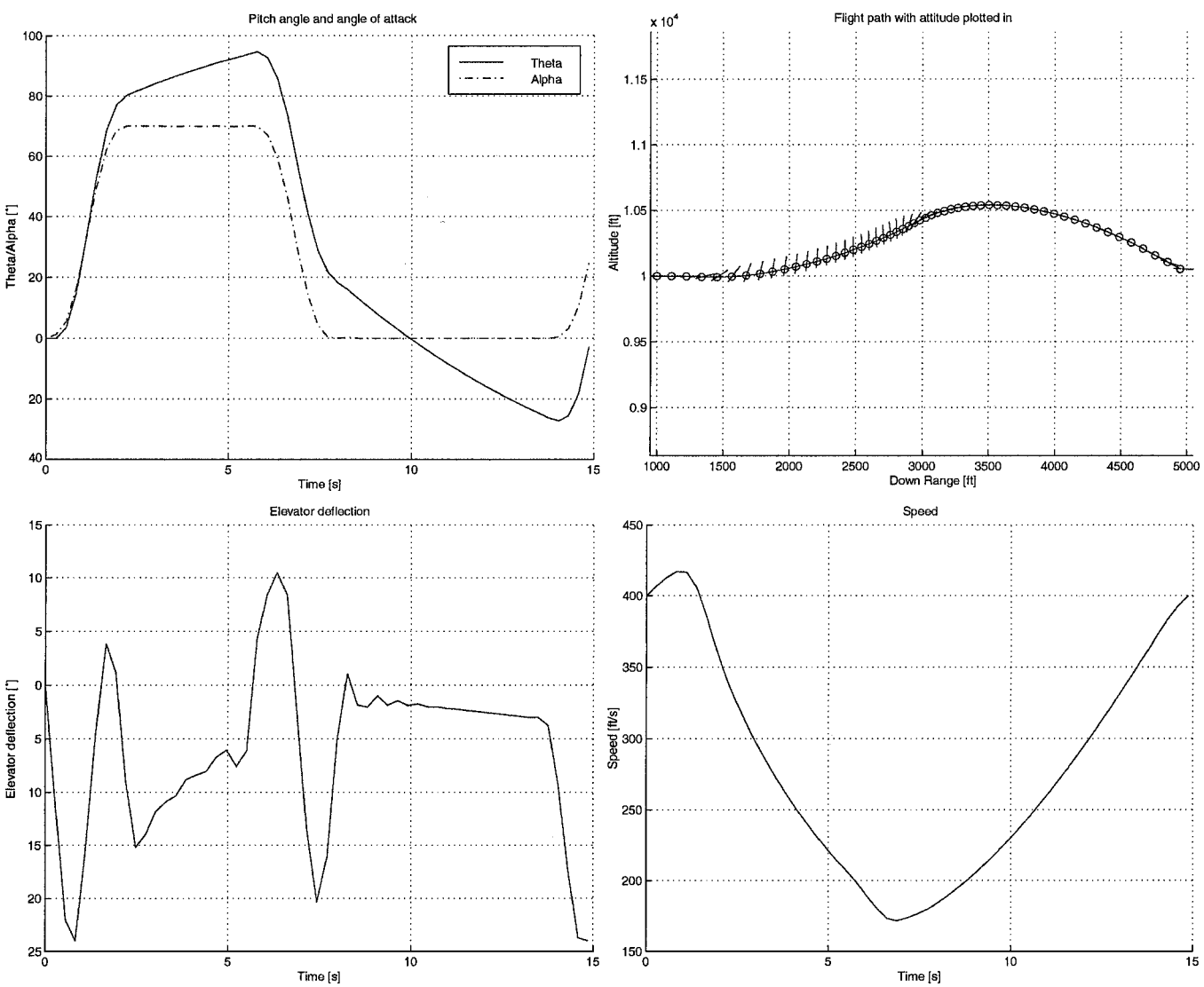

Fig. 5 Evader–pursuer maneuver, pointing, total distance, and final speed constraints.

$$C_l = C_{l\delta r}(\alpha)\delta_r + C_{l\delta a}(\alpha)\delta_a + C_{l\delta e}(\alpha)\delta_e + C_{l\beta}(\alpha)\beta + (b/2V)[C_{lp}(\alpha)p + C_{lr}(\alpha)r] \quad (37)$$

$$C_m = C_{m0}(\alpha, \delta_e) + (\bar{c}/2V)C_{mq}(\alpha)q + T_Z l_X/\bar{q}S\bar{c} \quad (38)$$

$$C_n = C_{n\delta r}(\alpha)\delta_r + C_{n\delta a}(\alpha)\delta_a + C_{n\delta e}(\alpha)\delta_e + C_{n\beta}(\alpha)\beta + (b/2V)[C_{np}(\alpha)p + C_{nr}(\alpha)r] - T_Y l_X/\bar{q}Sb \quad (39)$$

$$T_X = T_{\max} K(\delta_y, \delta_z)\cos\delta_y \cos\delta_z \quad (40)$$

$$T_Y = T_{\max} K(\delta_y, \delta_z)\sin\delta_y \cos\delta_z \quad (41)$$

$$T_Z = -T_{\max} K(\delta_y, \delta_z)\cos\delta_y \sin\delta_z \quad (42)$$

Gyroscopic moments produced by the engines and high body rates are not taken into account. The load factor is based on the normal force and is defined[4] as

$$n = (C_L \bar{q}S\cos\alpha + C_D \bar{q}S\sin\alpha + T\sin\delta_z)/Mg \quad (43)$$

The model used in this study is the NASA F-18 HARV. Data from several sources[8–10] were used to construct a model that is believed to be representative of the actual aircraft. The aerodynamic database is valid for $0 \le \alpha \le 70$ deg and $-30 \le \beta \le 30$ deg. Compressibility effects are neglected. The maximum load factor during the studied maneuvers always remained below the maximum value of 5.4 g (Ref. 11).

The restriction that the maneuvers take place in the vertical plane reduces the described six-DOF model to the following longitudinal model:

$$\dot{\alpha} = q - [\bar{q}SC_X/MV - (g/V)\sin\theta]\sin\alpha + [\bar{q}SC_Z/MV + (g/V)\cos\theta]\cos\alpha \quad (44)$$

$$\dot{q} = \bar{q}S\bar{c}C_m/I_{yy} \quad (45)$$

$$\dot{V} = (\bar{q}SC_X/M - g\sin\theta)\cos\alpha + (\bar{q}SC_Z/M + g\cos\theta)\sin\alpha \quad (46)$$

$$\dot{\theta} = q \quad (47)$$

$$C_X = C_L(\alpha, q, \delta_e)\sin\alpha - C_D(\alpha, \delta_e)\cos\alpha + T_X/\bar{q}S \quad (34)$$

$$C_Z = -C_L(\alpha, q, \delta_e)\cos\alpha - C_D(\alpha, \delta_e)\sin\alpha + T_Z/\bar{q}S \quad (36)$$

$$C_m = C_{m0}(\alpha, \delta_e) + (\bar{c}/2V)C_{mq}(\alpha)q + T_Z l_X/\bar{q}S\bar{c} \quad (48)$$

$$T_X = T_{\max} K(\delta_z)\cos(\delta_z) \quad (49)$$

$$T_Z = -T_{\max} K(\delta_z)\sin(\delta_z) \quad (50)$$

Verification of Optimal Trajectories

Lichtsinder et al.[6] showed that the simplification of constricting the movement of the aircraft to the vertical plane does not yield flight

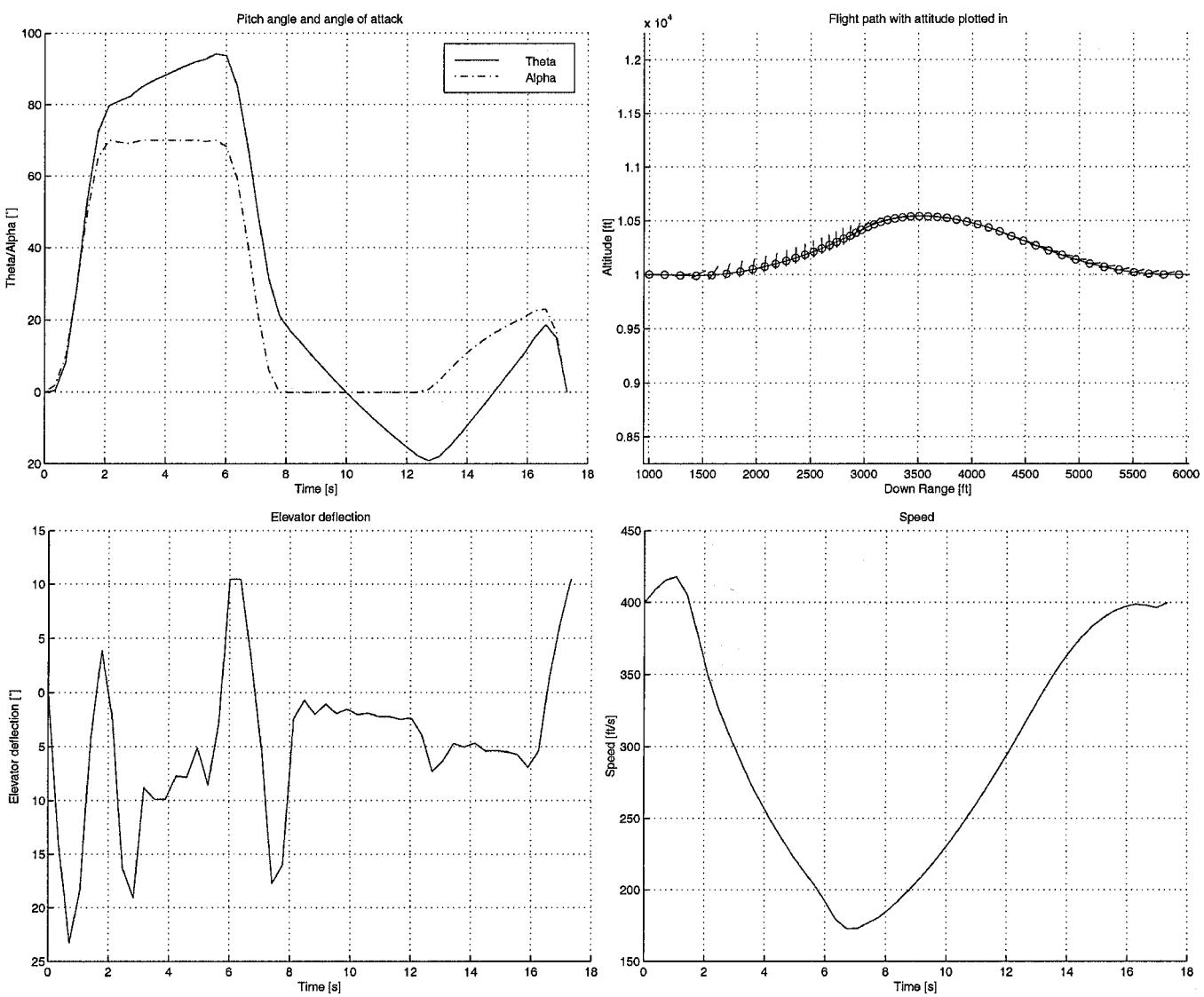

Fig. 6 Evader–pursuer maneuver, pointing, total distance, final speed, and final flight-path angle constraints.

paths that can be flown in real life. Asymmetric behavior of the aircraft at high AOA, which is due to asymmetric forebody vortices and a slight asymmetry in the aircraft (probes), gives rise to undesired banking- and heading-angle motions. Therefore, the flight path as obtained earlier, will be put in a simulator that utilizes nonlinear inversion closed-loop control in a complete six-DOF environment, to try and fly along the open-loop, vertical plane, optimal flight path. Because aircraft motion is no longer restricted to the vertical plane, the complete six-DOF model as presented in Eqs. (25–42) is used. The path resulting from this is considered to be the final (sub) optimal six-DOF trajectory.

The configuration of the nonlinear control laws used in this paper has been presented by Snell et al.[12] and was adapted to verify the optimal trajectories obtained through DOVNLPAC (Fig. 2). The trajectory controller used by Snell et al.[12] was replaced by the open-loop AOA history obtained during the optimization. The aerodynamic rolling angle was coupled to the course angle, to keep the aircraft on a straight flight path, that is, if the aircraft starts turning to the right, it will enter a left bank to bring the heading angle back to zero. Furthermore, the desired sideslip angle is kept at zero throughout the maneuver.

Numerical Results

The numerical results have been obtained by using a nonlinear programming and collocation technique.[13] This technique has been implemented in an in-house developed program called DOVNLPAC. The step size for the optimization was chosen as small as possible. This was done to capture the fast dynamics of the maneuvers. Too large a step size would result in spiky behavior of pitch rate and control variables. Decreasing step size means increasing the time needed for computations and increasing the total number of variables and boundary conditions. There is an upper limit to the number of variables and boundary conditions the program can handle (about 1000 variables plus boundary conditions), and so this also affects minimum step size. The limit on the number of variables is also the reason why elevator and TV deflections were coupled and not introduced as separate control variables.

Results on the evader–pursuer form of the cobra maneuver with the horizontal distance constraint (9) only are presented in Fig. 3. It can be seen that the AOA quickly saturates to its maximum value of 70 deg. Any further increase in pitch beyond this point comes from an increase in flight-path angle. Increase in altitude during the maneuver is slightly more than 650 ft. Maximum gravitational acceleration load is about 4.8g. The control history shows definite peaks with which the pitching movement is started, stopped, and reversed. Minimum speed is 138 ft/s, and the final speed is 190 ft/s. Total distance traveled during the maneuver is 2600 ft, and the total time needed to complete the maneuver is 11.5 s.

When the pointing constraint (11) is introduced (Fig. 4), and the horizontal distance constraint (4) is replaced by total distance constraint (12), the total maneuvering time increases to 13.05 s, and the final speed increases to 323 ft/s. This because the minimum speed is slightly higher at 167 ft/s and because during the pointing phase the initial evader starts to swoop down on the initial pursuer.

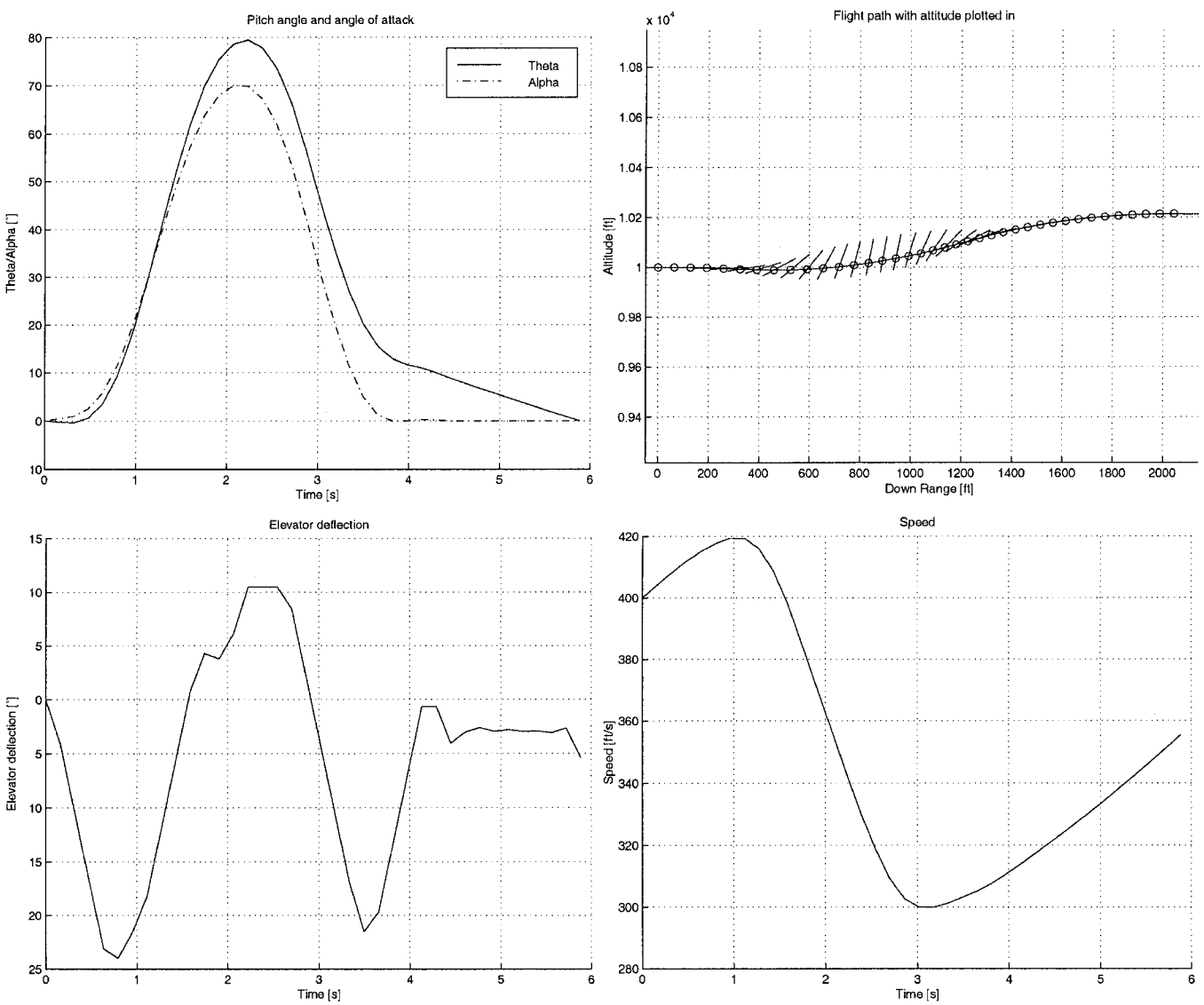

Fig. 7 Cobra maneuver as a max–max problem.

This swooping maneuver is utilized even further when the constraint that the final speed is 400 ft/s [Eq. (13)] is also introduced (Fig. 5). The final time increases to 14.87 s. The minimum speed increases to 171 ft/s. At the end of the maneuver, the aircraft increases its AOA to about 23 deg to point its nose toward the initial pursuer.

In the final evader–pursuer maneuver, the final value of the flight-path angle has been set to zero [Eq. (14)] (Fig. 6). The resulting maneuver is very similar to the preceding one. The total maneuvering time increases to 17.3 s. Minimum speed is 173 ft/s. The main difference between this maneuver and the preceding one is the final stage. In this case, the aircraft starts increasing AOA somewhat earlier to arrest its descent and to bring the flight-path angle to zero. That the aircraft returns to exactly the same altitude is because, due to the restrictions in the permissible AOA range [Eq. (24)], it is impossible to fly above the initial pursuer and still point the nose of the aircraft toward the initial pursuer.

In all cases, the maneuvering times are longer than those found by Horie and Conway.[5] This could be because a different type of aircraft is used (F-16-like aircraft vs F-18 HARV) but is probably because a rigid-body model was used in this investigation. Horie and Conway had no restriction on the initial AOA and used a thrust-to-weight ratio of precisely one. This enabled their maneuvering aircraft to start the maneuver at its initial speed of 400 ft/s, while having an AOA of 90 deg and a flight-path angle of 0 deg. As $T = W$ in their case, having an AOA of 90 deg also implies that the aircraft remains flying along a precisely horizontal flight path. After the aircraft has shed enough speed (by flying horizontally at 90-deg AOA), it pitches down. At that point, the aircraft starts descending and ends up below the initial pursuer. Near the end of the maneuver, it points its nose toward the initial pursuer.

This is completely different from the six-DOF trajectories presented here. For the aircraft used in this study, the thrust-to-weight ratio with no vectoring of thrust is not equal to one. Furthermore, the aircraft is unable to stand on its tail instantaneously. Therefore, the aircraft does not fly horizontally while flying at 90-deg AOA but starts climbing at high AOA. This results in the trajectories where the initial pursuer passes under the maneuvering aircraft instead of above it (as in Horie and Conway's trajectories[5]).

Results on the 80-deg pitch reversal maneuver can be seen in Fig. 7. The time needed to complete the maneuver is 5.88 s. Minimum speed during the maneuver is 300 ft/s.

Results on the closed-loop simulation of the maneuvers utilizing nonlinear inversion control are shown in Fig. 8. All maneuvers have been put through the simulator, but for the sake of brevity only the results on the evader–pursuer maneuver with pointing, total distance, final speed, and final flight-path angle constraints are shown. The results show that using the conventional aerodynamic control surfaces and longitudinal and lateral TV the trajectories obtained through DOVNLPAC could be flown quite accurately. Undesired roll and yaw movements were kept in check using small deflections of rudder, aileron, and lateral thrust deflection. There is a slight delay throughout the maneuvers, yielding slightly longer maneuvering

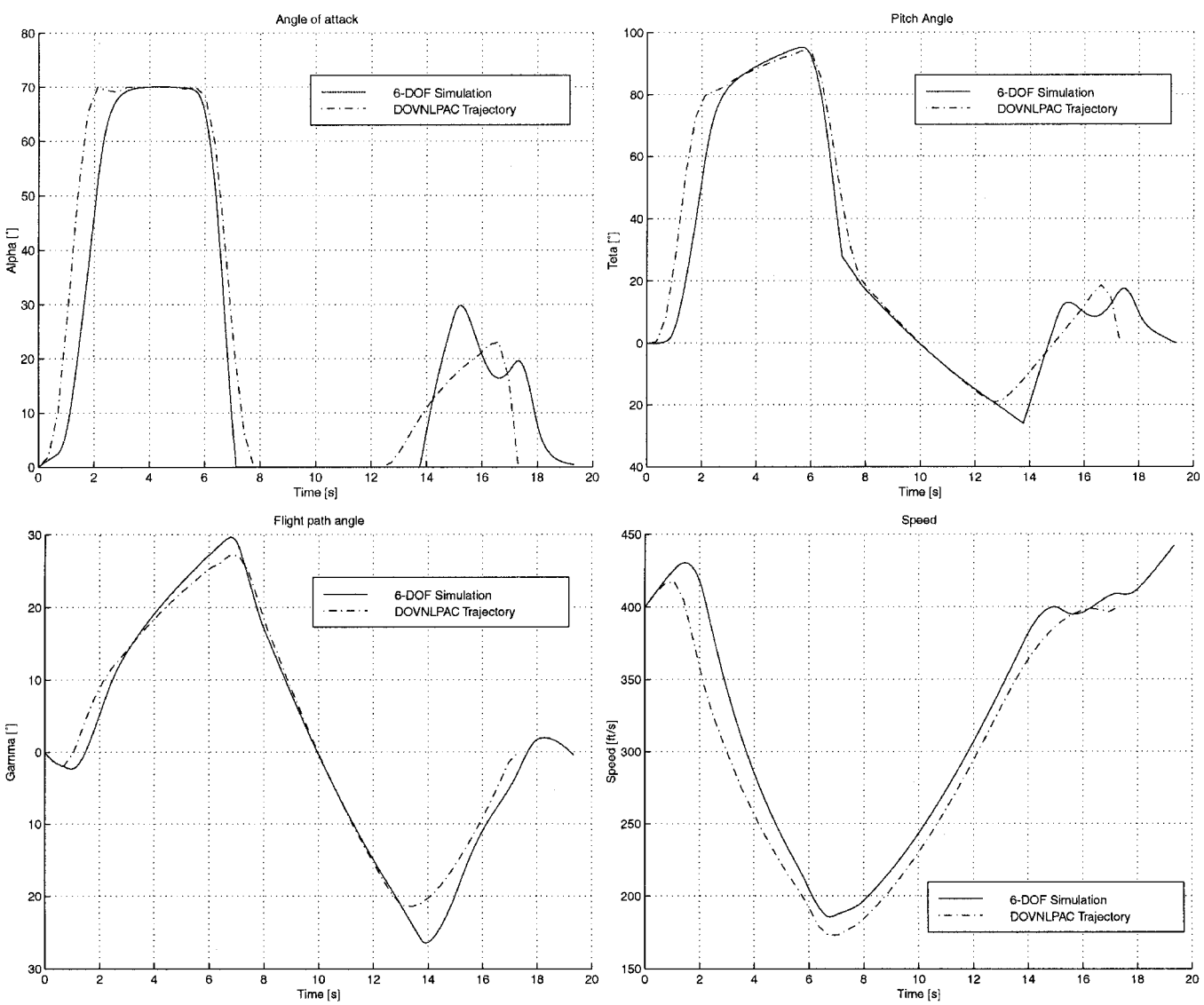

Fig. 8 Results of the six-DOF simulation of the evader–pursuer maneuver, with pointing, total distance, final speed, and final flight-path angle constraints.

times (in the case shown in Fig. 8 from 17.3 to 19.3 s). Because of the slight delay in AOA response at the beginning of the maneuver, airspeed remains a bit higher throughout the maneuver. This in turn causes the flight-path angle to grow somewhat faster. Therefore, maximum pitch angle is reached about 0.1 s earlier than in the optimal solution. Because the simulation uses pitch angle as a reference for how far along the optimal trajectory the aircraft is, this means that the aircraft starts to pitch down about 0.1 s earlier, too. This does not mean, however, that the simulated six-DOF trajectory is better than the vertical plane optimal trajectory because the aircraft has already traveled farther in the high AOA phase, due to the higher airspeed. During the simulation, the horizontal elevator and longitudinal TV vanes moved independently from one another. As expected, this shows that the linear relation used during the optimization phase is too simplistic. The six-DOF model shows the tendency to utilize the horizontal elevator at low angles of attack

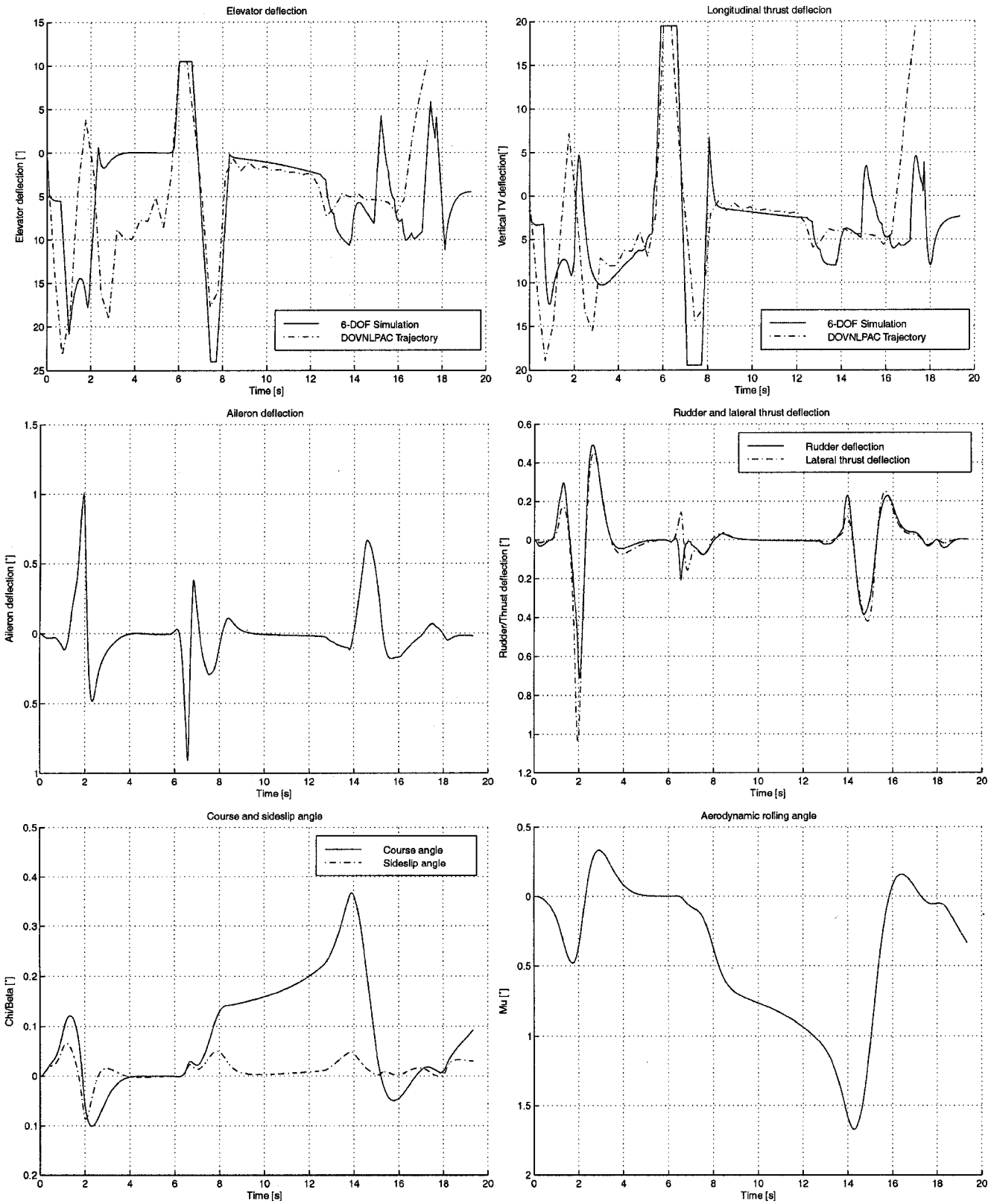

Fig. 8 Results of the six-DOF simulation of the evader–pursuer maneuver, with pointing, total distance, final speed, and final flight-path angle constraints (continued).

(Fig. 8; 0–2 s) and longitudinal TV at high angles of attack (Fig. 8; 2–6 s), where the effectiveness of the elevator is small. There also appears to be a relation with the airspeed (reduced effectiveness of aerodynamic control surfaces at low speed). One way of implementing this in the optimization is decoupling TV and deflections of the elevator and introducing each as a separate control variable. However, this currently produces problems with the maximum number of variables that can be handled during the optimization.

Conclusions

It has been shown to be feasible to optimize cobralike pitch reversal maneuvers while using a rigid-body model. The optimal trajectories were obtained for a number of terminal constraints using a nonlinear programming and collocation method.

For future study, decoupling longitudinal TV and horizontal elevator movement may be considered. Furthermore, the use of a smaller step size during the optimization may yield somewhat smoother control histories and may refine the final results. However, currently both improvements would produce problems with the maximum number of variables that can be handled during the optimization.

References

[1]Scott, W. B., "X-31 Kill Ratios Exceed Predictions," *Aviation Week and Space Technology*, Vol. 141, No. 6, 1994, pp. 54, 55.

[2]Fink, D. E., "Agile Sukhoi Su-27 Leads Strong Soviet Presentation," *Aviation Week and Space Technology*, Vol. 130, No. 24, 1989, pp. 28–30.

[3]Gal-Or, B., and Baumann, D., "Mathematical Phenomenology for Thrust-Vectoring-Induced Agility Comparisons," *Journal of Aircraft*, Vol. 30, No. 2, 1993, pp. 248–254.

[4]Murayama, K., and Hull, D. G., "The Cobra Maneuver as a Minimum Time Problem," AIAA Paper 97-3586, 1997.

[5]Horie, K., and Conway, B. A., "Optimization for Fighter Aircraft Vertical-Plane Maneuvering Using Poststall Flight," *Journal of Aircraft*, Vol. 37, No. 6, 2000, pp. 1017–1021.

[6]Lichtsinder, A., Kreindler, E., and Gal-Or, B., "Minimum-Time Maneuvers of Thrust-Vectored Aircraft," *Journal of Guidance, Control, and Dynamics*, Vol. 21, No. 2, 1998, pp. 244–250.

[7]Miele, A., and Wang, T., "An Elementary Proof of a Functional Analysis Result Having Interest for Minimax Optimal Control of Aeroassisted Orbital Transfer Vehicles," Rice Univ., Aero-Astronautics Rept. 182, Houston, TX, 1985.

[8]Bowers, A. H., and Pahle, J. W., "Thrust Vectoring on the NASA F-18 High Alpha Research Vehicle," NASA TM 4771, 1998.

[9]Hoffman, E., and Stalford, H., "Classical Turning Performance of a Fighter Aircraft Revisited," AIAA Paper 91-2669, 1991.

[10]Iliff, K. W., and Wang, K. C., "Flight-Determined, Subsonic, Lateral-Directional Stability and Control Derivatives of the Thrust-Vectoring F-18 High Angle of Attack Research Vehicle (HARV), and Comparisons to the Basic F-18 and Predicted Derivatives," NASA TP-1999-206573, 1999.

[11]Regenie, V., Gatlin, D., Kempel, R., and Matheny, N., "The F-18 High Alpha Research Vehicle: A High-Angle-of-Attack Testbed Aircraft," AIAA Paper 92-4121, 1992.

[12]Snell, S. A., Enns, D. F., and Garrard, W. L., "Nonlinear Inversion Flight Control for Supermaneuverable Aircraft," *Journal of Guidance, Control, and Dynamics*, Vol. 15, No. 4, 1992, pp. 976–984.

[13]Enright, J. E., and Conway, B. A., "Discrete Approximations to Optimal Trajectories Using Direct Transcription and Nonlinear Programming," *Journal of Guidance, Control, and Dynamics*, Vol. 15, No. 4, 1992, pp. 994–1002.